

Site selective electron paramagnetic resonance study of photoexcited chromium doped forsterite

Ayelet Regev and Jack H. Freed^{a)}

Baker Laboratory of Chemistry, Cornell University, Ithaca, New York 14853-1301

(Received 15 May 1995; accepted 30 June 1995)

Time resolved electron paramagnetic resonance (EPR) measurements on a photoexcited chromium doped forsterite (Cr:Fo) single crystal are reported. The spectral changes with time, magnetic field, crystal orientation, microwave power and, in particular, photoexciting wavelength, provide a selective picture of the various chromium dopants and the absorption-relaxation cycle associated with each optical excitation. Both Cr⁺⁴ ions lodged at tetrahedral (Td) and octahedral (Oh) sites as well as Cr⁺³ ions are detected. In particular, the laser-EPR technique enabled us to monitor the spin dynamics associated with the lasing center (Cr⁺⁴/Td) in the time regime of 200 ns–100 ms following a selective photoexcitation of the crystal between 532 and 1064 nm. The transient EPR signals associated with the lasing Cr⁺⁴/Td ions, exhibit a noticeable dependence on even small changes (~0.5 nm) in the exciting wavelengths that correspond to the visible $^3A_2 \rightarrow ^3T_1$ and the near infrared $^3A_2 \rightarrow ^3T_2$ transitions. The transient magnetization associated with each absorption-relaxation cycle is quantitatively analyzed in terms of site selectivity due to the narrow band (i.e., low intensity) microwave detection following a narrow band optical excitation. Given this observed selectivity, it is suggested that laser-EPR may be employed to study intersite interactions and site structure versus optical function relationships in forsterite as well as other solids doped with transition metal ions. © 1995 American Institute of Physics.

I. INTRODUCTION

Tunable solid state lasers, such as chromium doped forsterite (Cr:Fo), derive their broad luminescence and absorption bands from the interaction between the doped transition metal ion and the crystal field. However, owing mainly to this interaction the optical spectra of such lasers often lack the resolution required for diagnostic characterizations like dopants and sites determination. It is not surprising though, that electron paramagnetic resonance (EPR) has had an important role in recognizing the unique lasing center in Fo as Cr⁺⁴ ions substituting, as believed, Si⁺⁴ ions in tetrahedral sites.^{1–3} Further, EPR studies indicated an inhomogeneity in the tetrahedral sites, which was attributed to distortions induced by the chromium insertion.⁴ Considering the complexity of the forsterite system we further aim to establish a specific correlation between the excited lasing states and the EPR signals, and to closely monitor the spin dynamics associated with the lasing action by applying time-resolved optical EPR techniques. The EPR of photoexcited systems (laser-EPR) introduces a time-resolved detection of short-lived paramagnetic species in various spin states.^{5,6} In addition, this technique often provides valuable information on transient phenomena such as spin polarization and coherency, and enables magnetophotoselectivity.^{5,6} Thus, laser-EPR may serve as a complementary method whenever the optical techniques result in broad overlapping signals which make it difficult to identify the various species involved in complex systems such as Fo. Time-resolved direct detection EPR studies of excited states in transition metal ions are virtually nonexistent and would be expected to be especially challeng-

ing considering the number of the paramagnetic levels in Cr:Fo, and their fast relaxation rates, especially since some of them are fluorescent.^{7,8}

In the present work we employed pulsed laser excitation combined with X-band EPR direct detection of a Cr:Fo single crystal at liquid helium temperature. This technique enabled us to monitor the spin dynamics associated with the lasing center in the time regime of 200 ns–100 ms following a selective photoexcitation of the crystal between 532 and 1064 nm. The technique also facilitates a selective transient detection of the other Cr species in Fo, very likely including light-induced Cr⁺⁴ ions occupying octahedral (Oh) sites which were not identified unambiguously by any other method.^{4,9} In other words, the characterization of the various Cr species by the laser-EPR method becomes feasible due to their completely different dependence on both the excitation wavelength, the detection time scales, and the microwave power. In particular, the transient EPR signals associated with the lasing Cr⁺⁴ ions lodged in tetrahedral (Td) sites, exhibit a conspicuous dependence on the exciting wavelength both in the visible and near-infrared (NIR) regions that correspond to the $^3A_2 \rightarrow ^3T_1$ and $^3A_2 \rightarrow ^3T_2$ optical transitions, respectively. The transient magnetization associated with each absorption-emission cycle is quantitatively analyzed in terms of the ability of the narrow band microwaves to selectively detect particular sites, following a narrow band optical excitation. (More precisely, by narrow band microwaves we refer to the weak microwave magnetic fields as discussed in Sec. III.)

In Sec. II we give experimental details. The theoretical model for analyzing the time-resolved optical EPR signals is given in Sec. III. The results and discussion are given in Sec. IV with a summary in Sec. V.

^{a)} Author to whom correspondence should be addressed.

II. EXPERIMENT

The Cr:Fo single crystal used in this study was grown by M. Higuchi (Department of Materials Science and Engineering, Cornell University), by the floating zone method in an atmosphere of 83% oxygen and 17% argon. The precursor powder of 0.01 Cr/Si was prepared by J. L. Mass (Department of Chemistry, Cornell University). The chromium concentration of the single crystal was 310 ppm ($4.26 \times 10^{18} \text{ cm}^{-3}$) as determined via a neutron activation analysis. The crystal appears green, blue, and purple when viewed along the *a*, *b*, and *c* crystallographic axes, respectively. The detailed description of the crystal growth and characterization was published elsewhere.^{10–13}

The Cr:Fo crystal ($9 \times 4 \times 2 \text{ mm}^3$) was mounted onto a Supersil quartz holder, with the crystal axis **a** (*Pbnm* notation) parallel (by eye) with the holder long axis. Rotation of the crystal about its **a** axis allowed the external magnetic field, **B**, and the light propagation axis to be aligned in the **bc** plane. Thus, at zero rotation the crystal **b** axis is parallel to **B** and the laser light propagates parallel to the **c** axis. Most of the experimental data presented in this work was recorded while the angle between **b** and **B** was kept at 60° . At this orientation the *XY* transition of Cr^{+4}/Td has its resonance at about 1300 G, which is well separated from signals associated with the other dopants.

The temperature was maintained at 3 K, using a continuous flow cryostat (Oxford Instruments ESR 10). The crystal in the microwave cavity was photoexcited at the fundamental (1064 nm, $<1 \text{ cm}^{-1}$ bandwidth) and at the second harmonic (532 nm, $<0.2 \text{ cm}^{-1}$ bandwidth) of a Nd:YAG laser (Quanta Ray DCR-1A, repetition rate 10 Hz, $\sim 10 \text{ mJ/pulse}$). Photoexcitation at 550–900 nm ($<0.2 \text{ cm}^{-1}$ bandwidth) was carried out with a dye laser (Quanta Ray PDL-1) pumped by the second harmonic of the Nd:YAG. The excitation wavelengths correspond to transitions from the ground state, 3A_2 , into the 3T_2 and 3T_1 excited manifolds of Cr^{+4}/Td in forsterite.^{14,15}

Laser excitation time-resolved cw-EPR direct detection measurements were carried out on a Bruker ER-200D SRC spectrometer with the field modulation disconnected. The EPR signal was taken from the preamplifier just after the diode detector and fed into a digital oscilloscope (Tektronix TDS 520) synchronized with the laser.¹⁶ Kinetic traces from each magnetic field position were acquired and stored. The transient spectra at different times after the laser pulse and with respect to the external field were constructed from these kinetic profiles.¹⁶ By subtracting the signal prior to a laser pulse the contribution from any cw signal is removed. The repetition rate was adjusted so that the signal had returned to equilibrium prior to the next laser pulse. The spectra were compared, on-line, with the corresponding steady-state EPR spectra (with the field modulation connected) to confirm resonance positions and stability. Site selective spectra were acquired by fixing the magnetic field on one of the Cr^{+4}/Td resonance peaks at a certain orientation, while scanning the dye laser through a definite range and monitoring the transient magnetization obtained at each wavelength. The reproducibility of these excitation spectra was checked by employing various scanning rates and by scanning the dye laser

grid back and forth through the desired range. The excitation spectra were also compared with the distinctive kinetic traces acquired at each pumping wavelength.

III. TEMPORAL ANALYSIS

A. Qualitative description

Tentatively, the temporal behavior is described in terms of spin polarization and the excitation–emission cycles at each wavelength (cf. Fig. 1, Scheme I). This scheme reflects the effect of the crystal field variation among different subsets of ions on the inhomogeneous laser excitation. Such an effect was previously demonstrated for Cr^{+4} in forsterite by the occurrence of multiple lines in the NIR fluorescence line narrowing (FLN) spectra obtained via Zeeman optical measurements.^{3,17,18} Although the exact nature of the tetrahedral site distortion is not completely clear yet,^{4,15} we will adopt here the notation of C_{2v} orthorhombic distortion.¹⁵ The effect of the C_{2v} distortion is to split the excited states such that the second excited state, 3T_1 , for instance is split into 3A_2 , 3B_1 , and 3B_2 . Due to the spin–orbit interaction each triplet is further split into three components. The energy associated with the components of the first two excited states, namely; 3T_2 and 3T_1 , was estimated from the absorption site selective spectra, and is given in Refs. 14 and 15. It should be noted that according to the Tanabe–Sugano energy level diagram of Cr^{+4} ($3d^2$) in a tetrahedral crystal field, an excited 1E level, insensitive to the crystal field, is lying above the 3T_2 state at intermediate and low crystal field sites. The exact position of the 1E state with respect to the 3T_1 in the lasing centers of Cr:Fo is not clear yet, probably due to the low probability of the interconfigurational transition: $^3A_2 \rightarrow ^1E$. However, it is generally accepted that the 1E state is not higher than the 3T_1 state.^{14,15,19}

At 9.4 GHz we essentially detect a two-level system due to the large ZFS parameter $D = 64.26 \text{ GHz}$.⁴ Before the laser pulse, the system is thermalized, but upon firing the laser, the spin polarization emerges as a result of the selection rules associated with the optical pumping and the decay processes. According to Scheme I two main processes, direct and indirect, should be taken into account regarding the spin polarization and the evolution of the transient magnetization:

- (i) The direct depopulating process of the detected *X* and *Y* ground state sublevels: In the case considered in Scheme I, an immediate (on the EPR time scale) spin polarization emerges due to the selective photoexcitation to the higher triplet (3B_2) of the second excited state (3T_1).
- (ii) The delayed indirect populating process of the detected levels: Within a few nanoseconds after the laser excitation pulse, the photoexcited 3T_1 state relaxed nonradiatively to the lower excited triplet state (3T_2), and from there via fluorescence ($\tau_f \approx 30 \mu\text{s}$ at 10 K)^{15,20,21} or nonradiative processes back to the ground state. Therefore, according to this scheme the detected *X* and *Y* sublevels may be repopulated via at least six different such routes (possibly associated with different rates). The final detected population may have originated from two distinct sources, i.e., the original

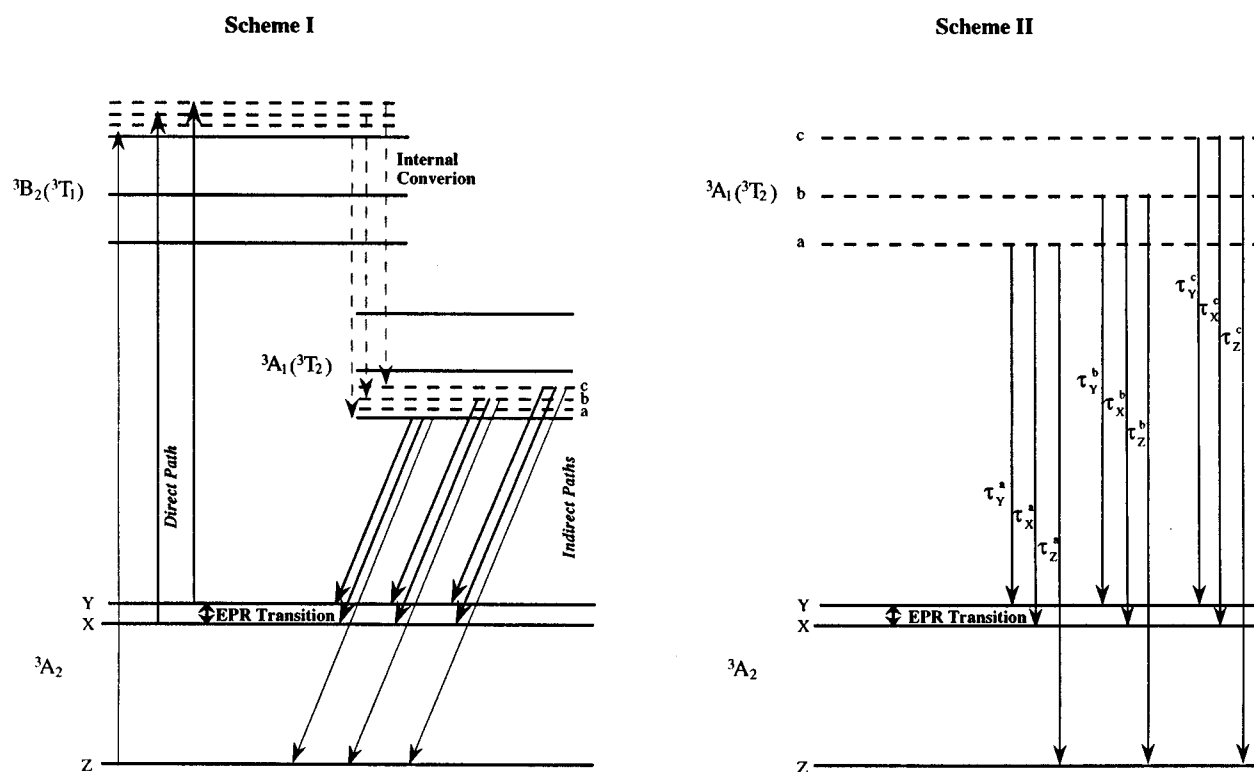


FIG. 1. Scheme I represents the excitation and decay cycles as detected by EPR following laser excitation (about 560 nm) of Cr^{+4}/Td ions doped in forsterite. The direct and indirect processes involved with the transient EPR signals are indicated. Scheme II is a simplified presentation of Scheme I, which describes the kinetic processes that occur at times longer than the laser excitation pulse (10 ns). The 1E level is not shown (cf. Sec. III).

X and Y sublevels, and also the Z ground state sublevel. It is anticipated that the effects of site variation in the ground state will mainly show up in the signals arising via the indirect process, since only this process will involve the Z level, which should be most sensitive to the crystal distortions.^{4,21,22} Due to the Boltzmann distribution at 3 K, which preferentially populates the ground Z level (since $D \sim 3$ K) the route originating from the Z ground state sublevel proceeding via the indirect process into the detected levels becomes even more important.

B. Quantitative description

Using Pedersen's modified Bloch equation formulation, the temporal behavior of the magnetization, $M(t)$, which includes spin relaxation and polarization effects as well as the optical relaxation, is given by²³

$$\dot{M}(t) = \mathbf{L}M(t) + \mathbf{F}(t), \quad (1)$$

where

$$\mathbf{L} = \begin{pmatrix} -T_2^{-1} & \Delta\omega & 0 \\ -\Delta\omega & -T_2^{-1} & -\omega_1 \\ 0 & \omega_1 & -T_1^{-1} \end{pmatrix},$$

$$\mathbf{F}(t) = \begin{pmatrix} 0 \\ 0 \\ f(t) \end{pmatrix},$$

and $f(t)$ depends essentially on the instantaneous spin concentration, $n(t)$, and will be discussed in detail below. All the other terms have their usual meaning. Formally, Eq. (1) is similar to the case of "slow radical decay" of Pedersen and hence can be solved by separating the magnetic and kinetic effects by the use of a Laplace transformation.²³ Therefore, for the short laser pulse case, i.e., $\tau_{\text{pulse}} \ll T_1$, there will be a nonequilibrium initial value of $M_z = m_0$, and the y component of M will be given by

$$M_y(t) = m_0 g_y(t) + f(t) * g_y(t), \quad (2)$$

where $g_y(t)$ is the solution of the magnetic part in Eq. (1) [i.e., when only the first term on the right-hand side of Eq. (1) is kept], and $f(t)$ represents the kinetics of the Cr:Fo according to Scheme I as discussed below. The asterisk in Eq. (2) implies a convolution. Given the observed oscillatory behavior of the transient magnetization of the Cr^{+4}/Td ions, the term $g_y(t)$ is given in terms of Torrey's underdamped solution of the Bloch equations²⁴

$$g_y(t) = -\frac{\omega_1}{\Omega} \exp(-bt) \sin(\Omega t), \quad (3)$$

where

$$b = \frac{1}{T_2} \left(1 - \frac{1}{2} \left(\frac{\omega_1}{\Omega} \right)^2 \right)$$

and

$$\Omega = \sqrt{\omega_1^2 + \Delta\omega^2},$$

and $\Delta\omega = \omega - \omega_0$, with ω the applied microwave frequency and ω_0 the resonance frequency. Implied in Eq. (3) is an assumption typical of the solid state that $T_1 \gg T_2$. Indeed, typical T_1 values for octahedral Cr^{+3} ions doped in various crystals at helium temperature are between 1 and 500 ms.²⁵ Our steady-state measurements on forsterite show that at the experimental temperature Cr^{+4}/Td is saturated at much lower microwave powers than even the Cr^{+3}/Oh . Thus, the temporal behavior of the transient magnetization should mainly depend on T_2 . Since the Cr^{+4}/Td signals return to equilibrium within a few milliseconds (T_1 mechanism) it could be safely assumed that $T_2 < 100 \mu\text{s}$. Assuming $T_2 > 1/2\omega_1$ (underdamping), the lower limit for T_2 is $0.7 \mu\text{s}$.

The actual expression for $f(t)$ could be obtained from the appropriate rate equations. Considering the relatively slow EPR time scale and neglecting any excited state absorption effects, Scheme I may be simplified as shown in Scheme II (Fig. 1). According to Scheme II at $t = \tau_{\text{pulse}} \approx 0_+$ both the ground and the lasing state sublevels are spin polarized. These spin polarized populations depend on the initial Boltzmann factors of the ground state sublevels, the relevant transition probabilities for absorption, and the relevant internal conversion rates. Therefore, the rate equation for the indirect path populating the p th ground state from the q th excited state sublevel is given by

$$\dot{n}_p(t) = \sum_q k_p^q n_q(t), \quad (4a)$$

where the depopulation of the q th lasing state sublevel is given by

$$\dot{n}_q(t) = -\left(\sum_p k_p^q\right) n_q(t) \equiv -k_T^q n_q(t), \quad (4b)$$

where $k_p^q = 1/\tau_p^q$. The solution of Eq. (4b) is

$$n_q(t) = n_q(0) \exp(-k_T^q t), \quad (5)$$

and the rate at which the buildup of the population difference for the EPR detected X - Y transition occurs is

$$f(t) \equiv \dot{n}_Y(t) - \dot{n}_X(t) = \sum_q n_q(0) (k_Y^q - k_X^q) \exp(-k_T^q t). \quad (6)$$

Inserting Eq. (6) into Eq. (2) we get

$$M_y(t) = m_0 g_y(t) + \sum_q g_y(t) * [n_q(0) (k_Y^q - k_X^q) \exp(-k_T^q t)]. \quad (7)$$

Since the various preexponential parameters in Eq. (7) are indistinguishable experimentally, the transient magnetization will be calculated according to

$$M_y(t) \equiv m_0 g_y(t) + \sum_q g_y(t) * [A_q \exp(-k_T^q t)]. \quad (7')$$

The typical linewidth in solid state EPR is often comparable to or even larger than the microwave field \mathbf{B}_1 . In such a case the microwave irradiation is often considered as a

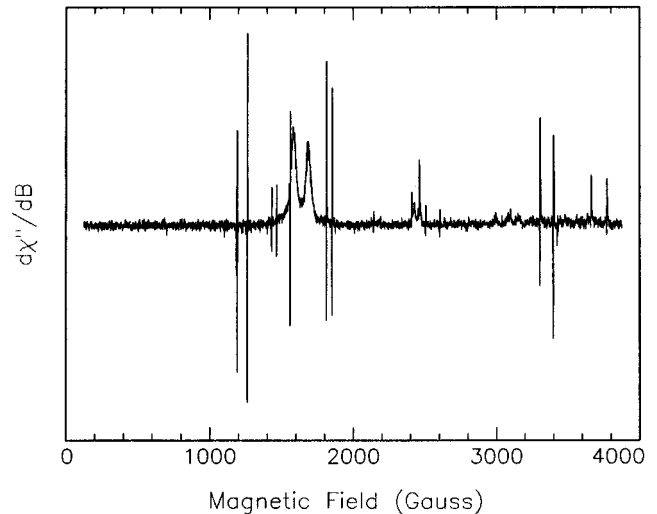


FIG. 2. First harmonic representation ($d\chi''/dB$) of a typical cw spectrum of Cr:Fo single crystal oriented with its \mathbf{b} axis rotated 70° from the external magnetic field, \mathbf{B} at 3 K. Field modulation 100 kHz, modulation amplitude 1 G, field scanning time 200 s and time constant $160 \mu\text{s}$.

narrow band excitation over the broadened line, and the expression for the transient magnetization may be obtained by summing over all contributions^{24,26}

$$I(t) = \int_{-\infty}^{\infty} h(\omega_0) M_y(t, \omega_0) d\omega_0, \quad (8)$$

where $h(\omega_0)$ represents the cw spectral lineshape, and that $M_y(t, \omega_0)$ depends on ω_0 via $\Delta\omega = \omega - \omega_0$. The exact effect of inhomogeneity depends however, on the particular lineshape. In the limit of a very large linewidth and excluding very short times, i.e., $\Omega t \gg 1$, an analytical solution was introduced via a damped Bessel function of zeroth order.^{24,26} Alternatively, the explicit lineshape, $h(\omega_0)$, can be inserted into Eq. (8) and $I(t)$ is then computed numerically. In the actual calculation the effects of site distribution on both the ground and excited states were further taken into account, as will be discussed in Sec. IV. The best fit procedure utilized a nonlinear minimization function that is based on a principal axis method.²⁷ In this way the gradients of the various functions were not required.

IV. RESULTS AND DISCUSSION

For a coherent presentation we first show a typical cw EPR spectrum of Cr:Fo at 3 K (Fig. 2). The spectrum consists of a broad signal located around 1700 G, which at the experimental crystal orientation is typical of Cr^{+4} ions located in tetrahedral (Td) sites, with narrower signals associated with the Cr^{+3} ions, as well as weaker unresolved signals. Due to the long spin relaxation times of the paramagnetic ground states at helium temperature such spectra suffer from saturation effects resulting in distorted absorption and dispersion signals which further complicate their analysis. However, the transient EPR spectra obtained via the optical EPR technique are quite different, as can be seen from Eq. (3).

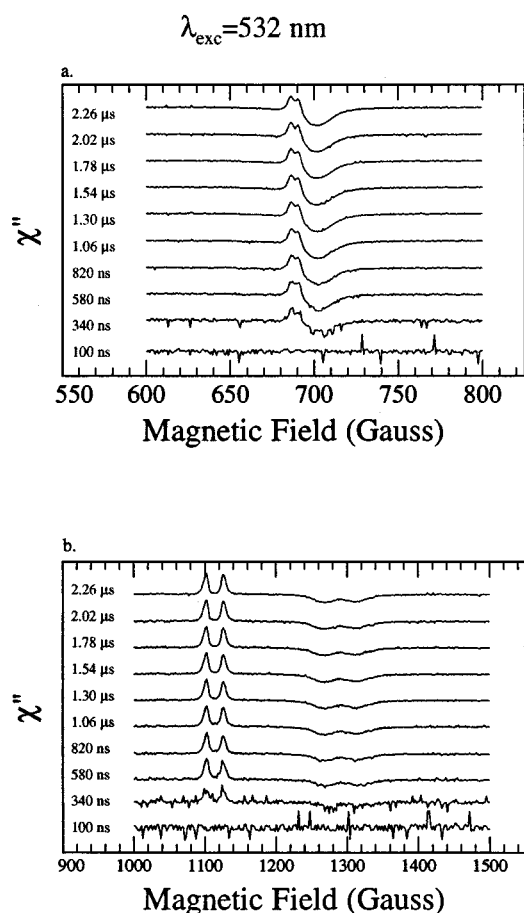


FIG. 3. Time evolved EPR spectra of Cr:Fo single crystal oriented with its **b** axis rotated 0° (a) and 60° (b) from the external magnetic field, **B** (cf. experimental) at 3 K. The spectra at 20 mW microwave power are an average of 20 (a) and 10 (b) kinetic traces obtained after the laser excitation pulse (10 ns, 10 mJ) at 532 nm.

A. Dopant selectivity

Figures 3 and 4 show the time evolution of the EPR spectra of Cr:Fo selectively excited at 532 and 1064 nm at two crystal orientations. These are much simpler spectra than the conventional steady-state ones observed at helium temperature (Fig. 2). In particular, the transient spectra only consist of signals associated with the optical excitation. Note that the absence of signal at 100 ns after the laser pulse is due to a combination of the dead time, and the natural time it takes to build up a transient nutation [cf. Eq. (3)]. The strong and broad signals observed at the higher fields [about 1300 G in Figs. 3(b) and 4(b)] and the higher field portion of the signal in Figs. 3(a) and 4(a) are associated with the Cr^{+4} lasing center. The signals at lower fields [around 1115 G in Figs. 3(b) and 4(b) and the lower field portion of the signal in Figs. 3(a) and 4(a)] are tentatively attributed to Cr^{+4} ions located at octahedral sites, due to their dependences on the temperature, microwave power, the crystal orientation with respect to the external magnetic field, and the exciting wavelength.²⁸ Comparison of cw spectra prior to and after laser irradiation, revealed that the signals attributed to Cr^{+4}/Oh are induced by the laser at low temperatures. However, once formed, these signals are persistent for even an

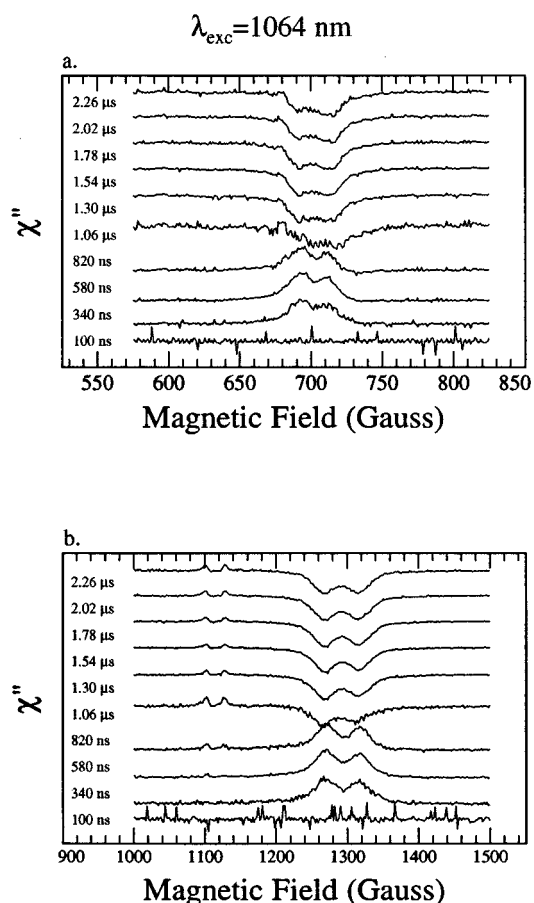


FIG. 4. Time evolved EPR spectra of Cr:Fo single crystal oriented with its **b** axis rotated 0° (a) and 60° (b) from the external magnetic field, **B** (cf. experimental) at 3 K. The spectra at 20 mW microwave power are an average of 10 kinetic traces obtained after the laser excitation pulse (10 ns, 10 mJ) at 1064 nm.

hour after the laser is turned off, and they disappear upon warming the sample to room temperature. In this paper we focus on the signals from the Cr^{+4}/Td ions, and the characterization of the other Cr^{+4} species will not be dealt with in this report. However, it is very clear from the figure that in addition to their different dependence on the crystal orientation they exhibit distinct dependence on the exciting wavelength. Whereas the signal associated with the Cr^{+4}/Td centers are stronger when employing NIR excitation ($\lambda=1064$ nm), those attributed to the Cr^{+4}/Oh ions are better detected following visible excitation ($\lambda=532$ nm). Moreover, the two types of signals are characterized with a different temporal behavior, as will be discussed below. On employing lower microwave power and longer detection times after the laser excitation pulse at 532 nm, the Cr^{+3} spectrum is obtained (not shown). In other words, the laser-EPR technique enables a selective transient detection, hence it facilitates the characterization of the various Cr species in forsterite, due to their distinctive dependence on the excitation wavelength, the detection time scales, and the microwave power.

B. Site selectivity

We shall confine our attention to the Cr^{+4}/Td lasing centers, for which the transient spectra reveal a noticeable de-

pendence of both the lineshape and the temporal behavior upon the exciting wavelength. Specifically, a phase inversion is detected about $1 \mu\text{s}$ after the laser pulse at 1064 nm, which is not observed at 532 nm. Such an inversion may imply an oscillatory behavior as is indeed expected under certain conditions from the transient magnetization following photoexcitation.²⁹ We attribute the oscillatory behavior observed at short times (within the first $2 \mu\text{s}$ after the laser pulse) to the direct depopulating mechanism, according to Eq. (3). Given, the lack of additional phase inversions, in spite of the weaker oscillations observed at longer times (not shown) this longer time behavior is ascribed to the delayed indirect populating process [cf. the second term in Eqs. (7)].

Previous cw EPR work indicated an inhomogeneity in the tetrahedral sites, which was attributed to distortions induced by the chromium insertion into the lattice.⁴ In order to relate the site distribution with the lasing tunability of Fo, and to exploit the selectivity of the laser-EPR technique, we monitored the dependence of the transient magnetization associated with the Cr^{4+}/Td ions upon the excitation wavelength. However, optical measurements had previously indicated that even a narrow band visible excitation to the second excited state of the lasing center did not yield line-narrowed fluorescence essential for the analysis of excitation-emission cycles.^{3,17,18} The observed broadening of the fluorescence was attributed to a loss of the site characterization during the nonradiative relaxation.^{3,30} We discuss below why we believe the optical EPR technique provides site selectivity.

In the present work the external magnetic field was fixed on one of the Cr^{4+}/Td resonance peaks, and the dependence of the transient magnetization on the exciting wavelength was monitored while scanning the wavelengths of the dye laser through the ${}^3A_2 \rightarrow {}^3B_2$, 3B_1 , ${}^3A_2({}^3T_1)$, and ${}^3A_2 \rightarrow {}^3B_2({}^3T_2)$ spectral ranges (Figs. 5, 6). Unlike the previous optical studies, a conspicuous dependence of the transient magnetization on the exciting wavelength is observed on exciting from the ground state level 3A_2 to either the 3B_2 or 3B_1 levels of the second excited electronic state, 3T_1 [Figs. 5(a) and 5(b), respectively]. The dependence on exciting to either the ${}^3A_2({}^3T_1)$ or ${}^3B_2({}^3T_2)$ levels is less noticeable but is evident with a careful examination [Figs. 6(a) and 6(b), respectively]. Similar measurements were carried out for the EPR signals associated with the other chromium species. Whereas the Cr^{4+}/Oh signals show some dependence upon the exciting wavelength, we could not detect any apparent wavelength dependence of the signals associated with Cr^{+3} ions that were detected for the longer times. It should be pointed out that the Cr^{+3} ions were not observed at short times (within $3 \mu\text{s}$) after the laser excitation pulse, possibly indicating that they are indirectly sensitized. However, we could not find any correlation between the wavelength dependence observed for the lasing center and the other chromium species that might imply any interaction between them within the detection time scales at 3 K. Alternatively, if Cr^{+3} transient nutation signals do not obey Eq. (3), i.e., they are overdamped, then the transient nutation could take longer to develop. Further measurements are required to fully address this issue.

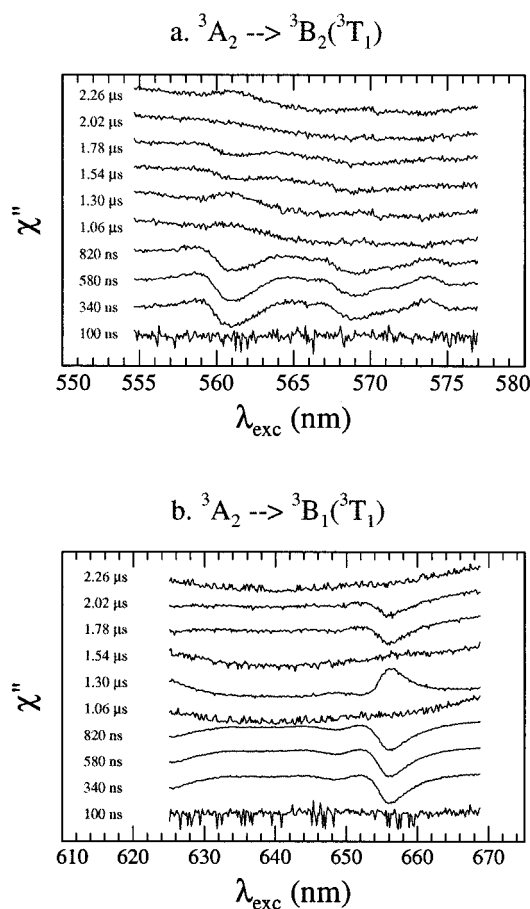


FIG. 5. Time evolved EPR spectra of Cr^{4+}/Td ions in forsterite photoexcited at two visible spectral regions according to the optical transitions (indicated) of the orthorhombic distorted tetrahedral sites (Ref. 15). The spectra, at 3 K and 80 mW microwave power, were recorded at the resonance field of the Cr^{4+}/Td (1426 G), when the crystal oriented with its **b** axis 60° from **B** and while scanning the dye laser grid with rates of: 0.09 (a) and 0.19 nm/s (b), and averaging 10 (a), 22 (b) kinetic traces at each wavelength.

The dependence of the transient magnetization associated with the lasing centers upon the optical exciting wavelength can be further studied by analyzing the temporal response of the magnetization at each wavelength (Fig. 7). It is evident from Fig. 7 that the dependence on the exciting wavelength is quite apparent even over the series that is shown, which for display purposes employs a very limited pumping range. In particular, a change of the excitation wavelength by less than a nanometer already manifests itself in the magnetic resonance response, as can be seen by comparing the profiles obtained at 572 nm ($1.748 \times 10^4 \text{ cm}^{-1}$) and 572.5 nm ($1.747 \times 10^4 \text{ cm}^{-1}$), i.e., a difference of $\sim 15 \text{ cm}^{-1}$ (Fig. 7). Thus, the laser-EPR technique introduces enhanced selectivity, and the relatively broadband laser excitation that was used ($\sim 0.2 \text{ cm}^{-1}$ bandwidth) is more than adequate. Combining this selectivity with the nutational behavior observed at the shorter times after the laser exciting pulse, provides one with a sensitive spectroscopic tool. For example, the phase inversion of the first nutation observed at 570 nm (Fig. 7), is indicative of an abrupt increase in the transition strength for absorption of the ground state sublevel

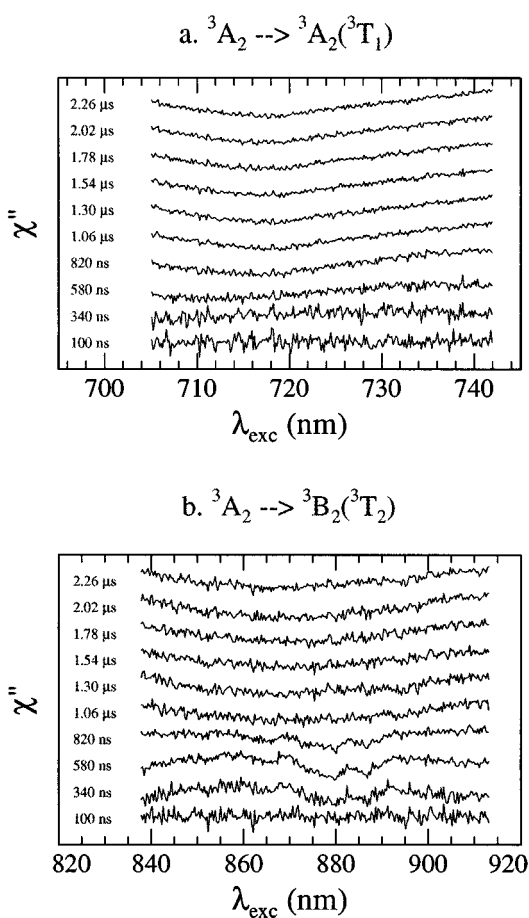


FIG. 6. Time evolved EPR spectra of Cr^{4+}/Td ions in forsterite photoexcited at a visible and a NIR spectral regions according to the optical transitions (indicated) of the orthorhombic distorted tetrahedral sites (Ref. 15). The spectra, at 3 K and 80 mW microwave power, were recorded at the resonance field of the Cr^{4+}/Td (1426 G), when the crystal oriented with its \mathbf{b} axis 60° from \mathbf{B} and while scanning the dye laser grid with rates of: 0.10 (a) and 0.19 nm/s (b), and averaging 36 (a) and 18 (b) kinetic traces at each wavelength.

X as compared to the absorption from the Y sublevel. It is tempting to assume that a mixing of the 3T_1 manifold with the close lying 1E level (in tetrahedral symmetry, cf. Sec. III) is responsible for the sudden phase inversion, especially given that such an inversion only occurs when exciting to the ${}^3B_2({}^3T_1)$ or ${}^3B_1({}^3T_1)$ levels, as can be seen in Fig. 5. Indeed, the energy of the 1E level was estimated to lie between the levels ${}^3B_2({}^3T_1)$ and ${}^3B_1({}^3T_1)$,^{14,15} and similar inversions were not detected when exciting either the ${}^3A_2({}^3T_1)$ or the ${}^3B_2({}^3T_2)$ levels.

Analogous to the FLN technique, which introduces selectivity due to a very narrow photoexcitation, the laser-EPR method must be gaining its selectivity from the narrow microwave detection. The obvious comparison between the optical and microwave source linewidths, e.g., the laser bandwidth of 10^{-2} cm^{-1} employed in FLN studies as compared to a microwave field of $\sim 10^{-5} \text{ cm}^{-1}$, could be expected to account for the enhanced resolution of the latter. Note that the laser bandwidth employed in the current site selective measurements, i.e., 0.2 cm^{-1} , must be adequate for exciting

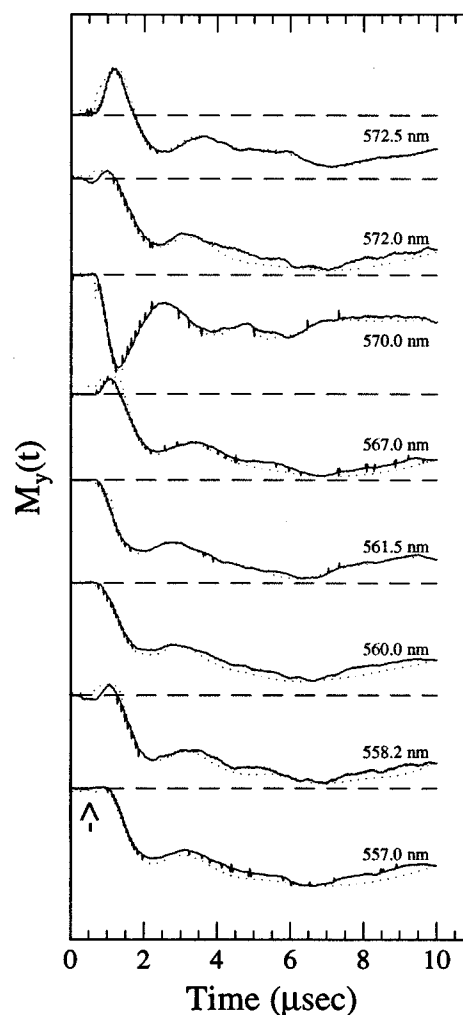


FIG. 7. Comparison of the temporal profiles of the magnetization, $M_y(t)$, of Cr^{4+}/Td ions in forsterite photoexcited to ${}^3B_2({}^3T_1)$ at different wavelengths (indicated). All other experimental conditions were kept constant: Temperature 3K; Magnetic field 1426 G; Microwave power 20 mW; Laser pulse: 10 ns, 10 mJ and bandwidth less than 0.2 cm^{-1} . Laser pulse position is indicated by an arrow. The dotted lines superimposed on the experimental traces (solid lines) are best fit results according Eq. (9) with the parameters T_2 , τ_T , and $\Delta\omega$ listed in Table I.

mainly one ground state sublevel at each site, since the ZFS between the XY levels is greater than 0.3 cm^{-1} .^{1,4} Thus, it is not surprising that the direct depopulating mechanism (optical excitation) is very site selective, as reflected by the phase inversion observed at short times. Nonetheless, the selectivity detected at longer times is less obvious and could easily be lost during the nonradiative relaxation between the 3T_1 and 3T_2 levels. Indeed, optical excitation of the 3T_1 and 3T_2 levels, employing the same bandwidth for both (or even a broader bandwidth for the 3T_2 level), yielded a FLN signal only when the 3T_2 level was directly pumped.^{1,3,17} It has been suggested that the loss of site characterization, when pumping the 3T_1 state and observing the nonresonant fluorescence from the 3T_2 level, could be either due to the increased linewidth associated with nonresonant vs resonant fluorescence, or due to energy migration between different sites.^{3,31} This extra linewidth is believed to arise from the

TABLE I. Best-fit values of the ground state magnetic parameters (T_2 and $\Delta\omega$) and excited state lifetimes (τ_i^q) of Cr^{+4}/Td ions photoexcited to the ${}^3B_2({}^3T_1)$ level at 20 mW microwave power. The $\tau_i^{q=b,c}$ ($i=1,4$) denote the τ_i^q parameters in Eq. (9) with $q=b$ or c and are presented in order of decreasing magnitude. The $\tau_i^{q=a}$ ($i=1,2$) denote the τ_i^q parameters in Eq. (9) with $q=a$, that were obtained using a Bessel function instead of $g_y(t)$, and are presented in decreasing order.

$\mu\text{s}/\text{nm}$	557	558.2	560	561.5	567	570	572	572.5
T_2	1.02	2.34	0.70	5.00	0.70	0.70	0.70	2.05
$\tau_1^{q=b \text{ or } c}$	29.76	30.74	1.79	32.33	28.07	0.97	32.15	36.98
$\tau_2^{q=b \text{ or } c}$	29.65	30.01	1.10	32.26	18.44	0.94	32.14	36.78
$\tau_3^{q=b \text{ or } c}$	16.28	18.15	0.99	4.06	18.42	0.32	4.67	1.87
$\tau_4^{q=b \text{ or } c}$	15.41	11.79	0.94	2.91	1.05	0.20	3.53	0.20
$\tau_1^{q=a}$	0.54	3.37	10.75	31.64	31.11	0.47	2.06	0.84
$\tau_2^{q=a}$	0.48	0.20	4.55	4.78	4.73	0.20	1.94	0.69
$\Delta\omega^a$	0.07	^b	0.11	^b	0.07	^b	0.06	^b

^aIn Gauss.

^bLess than 1% of the estimated $\mathbf{B}_1 \cdot \mathbf{B}_1$ was estimated considering a rectangular cavity with $Q \sim 1000$ (cf. caption of Fig. 6).

checked by assuming additional contributions from either several discrete sites or from a continuous distribution. The best fits were achieved by assuming at least two distinct contributing sites for each excited state sublevel with a small Gaussian distribution over their lifetimes and a broader Gaussian distribution of the relative contributions from each site. Thus, the best fit curves superimposed on the experimental traces in Fig. 7 are a result of computer optimization of the following expression derived from Eq. (7'):

$$I(t) = m_0 g_y(t) + \sum_q \left(g_y'(t) * \sum_{i=1,2} \int_{-\infty}^{\infty} G(A_{q_i}) \int_{-\infty}^{\infty} G(k_T^{q_i}) \times \exp(-k_T^{q_i} t) dA_{q_i} dk_T^{q_i} \right), \quad (9)$$

where

$$g_y'(t) = \begin{cases} g_y(t), & q=b,c \\ -\pi\omega_1 h(\omega_{MW}) J_0(\omega_1 t) \exp(-t/2T_2), & q=a \end{cases}$$

and $\int_{-\infty}^{\infty} G(v) dv$ represents a Gaussian distribution in v .

The parameters in Eq. (9) were restricted during the analysis to be within certain ranges. However, these ranges at best could only be estimated due to the lack of independent information about most of the parameters. The lower limit for the relaxation time T_2 was set according to the requirements presented in Eq. (3) for an oscillatory description of the transient magnetization at the lowest microwave power employed, i.e., $T_2 \geq 0.7 \mu\text{s}$. On the other hand, the only real restriction on the upper limit is that $T_1 \gg T_2$. Since all experimental transients decayed within a few milliseconds, we first arbitrarily set an upper limit of $T_2 \leq 100 \mu\text{s}$. However, since most of the actual values obtained via the NLS fitting correspond to $T_2 < 5 \mu\text{s}$, we later restricted the upper limit to $5 \mu\text{s}$. Twice the estimated rise time of the spectrometer, i.e., ~ 200 ns, was set as the lower limit of the time constants of the indirect processes, τ_p^q . Setting the upper limit for the rate of these processes needs some further considerations. Basically, the detailed kinetic analysis was carried out on the transients detected within the first $20 \mu\text{s}$ after the laser excitation pulse. However, strong transients could be detected over a more extended time scale up to a few milliseconds. The signals

observed in the millisecond time scale are similar to those reported previously by EPR relaxometry measurements.³³ Setting a few milliseconds as the upper limit for the indirect time constants yielded satisfactory fits. Inspection of the best-fit values obtained revealed though, a very wide range of lifetimes of the excited state sublevels, spanning indirect populating processes with rate constants between the lower limit (200 ns) through time constants on the order of the fluorescence lifetime measured at 10 K, i.e., $30 \mu\text{s}$,^{15,21} and up to a few milliseconds. A simple model of close-lying energy levels associated with neighboring sites (cf. Fig. 1) cannot reasonably account for such a wide range, especially at the limit of the very long times. Possible mixing of the 3T_1 levels with the closely lying 1E level could account for long lifetimes, due to the spin forbidden transition from E_1 to the ground state. We tend however to eliminate this explanation, since to the best of our knowledge optical measurements did not reveal any clear indication for a ${}^1E \rightarrow {}^3A_2$ transition, in spite of several reports on such transitions in other Cr^{+4} doped media.^{34,35} Moreover, it seems that the EPR signals we observed over the millisecond time scale at 3 K originate from Boltzmann equilibration (T_1 mechanism) together with possible saturation effects from the cw microwave field. Therefore the best fit results summarized in Table I were obtained after restricting τ_p^q to an arbitrary maximum value of $40 \mu\text{s}$. It should be pointed out that the fits were comparable to those obtained when the parameters were less restricted. The reasonable fits allow us to draw some qualitative conclusions.

Inspection of Table I shows two main ranges for the τ_p^q values. The best-fit results of the preexponential parameters A_q are not shown since we cannot separate the physically significant components of the A_q that appear in Eq. (7). The longer times (20–30 μs) shown in Table I, are in accordance with the fluorescence times reported at 10 K.^{15,21} However, additional processes associated with much shorter times (0.2–10 μs) seem to contribute frequently to the transient EPR traces. There are some indications of two types of NIR fluorescence, characterized by different lifetimes, in two other Cr^{+4}/Td doped crystals.^{36,37} In particular, time-resolved fluorescence measurements reveal a temporal dependence of the relative intensity of the zero phonon line and the spectral

structure observed at lower energy, following pumping of Cr:Fo at 532 nm.³⁶ Additionally, the luminescence observed after pumping at 1064 nm showed a nonexponential decay.³⁶ Such findings are in accordance with the additional higher rates found in the present work. Alternatively, the higher rates obtained via the temporal analysis may be associated with nonradiative processes, which may explain the weaker fluorescence yield reported for pumping the Cr:Fo at 532 nm as compared to 1064 nm, especially at high temperatures.^{36,38} The existence of long lifetimes of the excited states of the order of the radiative lifetimes may be indicative of very slow spectral diffusion between different sites, as was mentioned above. It is possible that spectral diffusion would be manifest for higher chromium concentrations and that this could be further addressed by laser-EPR measurements.

Despite the clear dependence of the nutational behavior upon the microwave power, the curve for each power was fitted separately. Unsatisfactory fits were obtained when trying to simultaneously minimize several experimental sets that were recorded under different microwave power following a similar optical excitation. This may suggest that the selectivity induced via the microwave irradiation may be reduced, e.g., higher powers sample more sites. For instance it was found that shorter T_2 values are required for fitting the transient magnetization profiles obtained under higher microwave power, e.g., $T_2=0.76$ and $2.26 \mu\text{s}$ for 80 and 8 mW, respectively. Another indication for site discrimination by the microwave detection is the different off resonance contributions, reflected by the $\Delta\omega$ parameter (Table I) that were found at each wavelength. Although most of the kinetic traces could be reasonably fit with negligible off resonance contributions, much better fits were sometimes obtained when allowing for excitations that were off resonance. However, we could not find any correlation between the $\Delta\omega$ values and the experimental microwave power as would be expected for a broad EPR line which consists of nonoverlapping contributions as mentioned above.

Finally, the advantage of utilizing two exciting paths for each ground state sublevel over employing one broad excitation, and the lack of substantial improvement when further increasing the number of paths deserve a few words. Measurements of effects of uniaxial stress on the NIR fluorescence of Cr:Fo demonstrated pseudospectral splitting into two groups, indicative of Cr^{+4} ions located in two equivalent sublattices.^{19,39} Those results further implied that the two sublattices are characterized with differently oriented dipoles, neither parallel to each other nor to any crystal axis.^{19,39} It might be expected that magnetophotoselection measurements, utilizing different light polarizations with respect to the crystallographic axes and the external magnetic field while detecting the transient nutation, would allow us to determine whether the two-site behavior observed in the present work is indeed related to the double sublattice structure. However, the preliminary measurements we have performed were not conclusive in that no significant effects were observed, possibly because of the crystal orientation used and/or the nonradiative relaxation processes involved, which could reduce the polarization effects. Careful magne-

tophotoselection measurements utilizing a range of crystal orientations may be required to address this point.

V. SUMMARY

This work shows the feasibility of transient EPR detection of photoexcited chromium doped forsterite. The spectral changes with time, magnetic field, crystal orientation, microwave power and in particular photoexciting wavelength, provide a selective picture of the various chromium dopants and the absorption-relaxation cycle associated with each optical excitation. Focusing on the lasing centers, small changes (less than a nanometer) in the exciting wavelength reversed the relative absorption cross section of the detected ground state sublevels, and was clearly reflecting changes in the decay of the excited states. The analysis, in its preliminary stages, related the changes in the transient EPR signals to variations in the tetrahedral sites of the Cr^{+4} ions, and provided radiative as well as nonradiative time constants associated with the emission of Cr:Fo. Moreover, it was shown that optical depopulation of the detected levels is a sensitive probe for the site selective ground state absorption. In that regard, laser-EPR complements the optical measurements of resonant FLN effects which involve weak spectral intensities due to the relaxation of the excited states being monitored.³ Similarly, the indirect repopulation processes as detected by EPR do not suffer from scattering effects associated with the pumping laser beam, which complicate the analysis in FLN studies.³ As to what extent laser-EPR measurements could be employed in studying chromium-chromium interaction between different sites, and in associating a specific site structure with the excited state decay, is a subject for more detailed and comprehensive studies. It is conceivable that the laser-EPR technique may be also applicable for other transition metal ions doped in optically active materials.

It could also be of value to employ spin-echo detection techniques to complement the transient nutation detection used in the present work.^{6,40,41} In this work both T_2 and the kinetic parameters were obtained from simultaneous least-squares fits. In spin-echo detection one can separate the T_2 measurement from that of the kinetic parameters. On the other hand, the transient nutation provides a time dependent signal from each laser pulse, whereas the usual spin-echo methods just give a single datum, viz. the echo height. Also, one must use very weak microwave pulses to preserve the site selectivity.

ACKNOWLEDGMENTS

We are grateful to Jennifer L. Mass and M. Higuchi for providing the Cr:Fo crystal used in this study. We also thank Jennifer L. Mass for kindly sharing with us any relevant information. It is a pleasure to thank Stephen P. Smith, of the facility for laser spectroscopy of the Chemistry Department, for his assistance in setting the lasers and the optics. We also acknowledge the assistance of Antonino Polimeno, David E. Budil, and Richard Crepeau. This work was supported by the Cornell Materials Science Center and by NSF Grant No. CHE-9313167. Computations were carried out at the Cornell

National Supercomputer Facility (CNSF) and at the computer facility of the Cornell Materials Science Center.

- ¹K. R. Hoffman, J. Casas-Gonzalez, S. M. Jacobsen, and W. M. Yen, *Phys. Rev. B* **44**, 12589 (1991).
- ²M. H. Whitemore, A. Sacra, and D. J. Singel, *J. Chem. Phys.* **98**, 3656 (1993).
- ³T. S. Rose, R. A. Fields, M. H. Whitemore, and D. J. Singel, *J. Opt. Soc. Am. B* **11**, 428 (1994).
- ⁴D. E. Budil, D. G. Park, J. M. Burlitch, R. F. Geray, R. Dieckmann, and J. H. Freed, *J. Chem. Phys.* **101**, 3538 (1994).
- ⁵S. S. Kim and S. I. Weissman, *Rev. Chem. Intermed.* **3**, 107 (1979).
- ⁶For recent reviews see for example: (a) H. Levanon and M. K. Bowman, in *The Photosynthetic Reaction Center*, edited by J. Deisenhofer and J. R. Norris (Academic, San Diego, 1993), Vol. II, p. 387; (b) K. A. McLaughlan, in *Modern Pulsed and Continuous-Wave Electron Spin Resonance*, edited by L. Kevan and M. K. Bowman (Wiley, New York, 1990); (c) D. Stehlik, C. H. Bock, and M. C. Thurnauer, in *Advanced EPR Applications in Biology and Biochemistry*, edited by A. J. Hoff (Elsevier, New York, 1989), p. 371.
- ⁷S. Geshwind, in *Electron Paramagnetic Resonance*, edited by S. Geshwind (Plenum, New York, 1972), p. 353.
- ⁸O. G. Poluektov, M. C. J. M. Donckers, P. G. Baranov, and J. Schmidt, *Phys. Rev. B* **47**, 10226 (1993).
- ⁹J. Casas-Gonzalez, S. M. Jacobsen, K. R. Hoffman, and W. M. Yen, in *OSA Proceedings on Advanced Solid State Lasers*, edited by G. Dube and L. Chase (Optical Society of America, Hilton Head, SC, 1991), Vol. 10, p. 64.
- ¹⁰J. L. Mass, J. M. Burlitch, D. E. Budil, J. H. Freed, D. B. Barber, C. R. Pollock, M. Higuchi, R. F. Geray, and R. Dieckmann, *Chem. Mater.* **7**, 1008 (1995).
- ¹¹D. G. Park, J. M. Burlitch, R. F. Geray, R. Dieckmann, D. B. Barber, and C. R. Pollock, *Chem. Mater.* **5**, 518 (1993).
- ¹²J. M. Burlitch, M. L. Beeman, B. Riley, and D. L. Kohlstedt, *Chem. Mater.* **3**, 692 (1991).
- ¹³M. Higuchi, R. F. Geray, R. Dieckmann, D. G. Park, J. M. Burlitch, D. B. Barber, and C. R. Pollock, *J. Cryst. Growth* **148**, 140 (1995).
- ¹⁴V. Petricevic, S. K. Gayen, and R. R. Alfano, in *OSA Proceedings, on Tunable Solid State Lasers*, edited by M. L. Shand and H. P. Jensen (Optical Society of America, Cape Cod, MA, 1989), Vol. 5, p. 77.
- ¹⁵W. Jia, H. Liu, S. Jaffe, W. M. Yen, and B. Denker, *Phys. Rev. B* **43**, 5234 (1991).
- ¹⁶O. Gonen and H. Levanon, *J. Phys. Chem.* **89**, 1637 (1985).
- ¹⁷K. R. Hoffman, S. M. Jacobsen, J. Casas-Gonzalez, and W. M. Yen, in *OSA Proceedings on Advanced Solid State Lasers*, edited by G. Dube and L. Chase (Optical Society of America, Hilton Head, SC, 1991), Vol. 10, p. 44.
- ¹⁸T. S. Rose, R. A. Fields, M. H. Whitemore, and D. J. Singel, in *OSA Proceedings on Advanced Solid State Lasers*, edited by L. Chase and A. A. Pinto (Optical Society of America, Santa Fe, NM, 1992), Vol. 13, p. 17.
- ¹⁹W. Jia, H. Liu, Y. Wang, U. Hömmerich, H. Eilers, K. Hoffman, and W. M. Yen, *J. Lumin.* **59**, 279 (1994).
- ²⁰T. J. Carrig and C. R. Pollock, in Ref. 9, Vol. 10, p. 72.
- ²¹R. Moncorge, D. J. Simkin, G. Cormier, and J. A. Capobianco, in Ref. 14, Vol. 5, p. 93.
- ²²H. Rager and G. Weiser, *Bull. Miner.* **104**, 603 (1981).
- ²³J. B. Pedersen, *J. Chem. Phys.* **59**, 2656 (1973).
- ²⁴H. C. Torrey, *Phys. Rev.* **76**, 1059 (1949).
- ²⁵K. J. Standly and R. A. Vaughan, *Electron Spin Relaxation Phenomena in Solids* (Plenum, New York, 1969), Chap. 9 and pp. 201–205.
- ²⁶R. Furrer, F. Fujara, C. Lange, D. Stehlik, H. M. Vieth, and W. Vollmann, *Chem. Phys. Lett.* **75**, 332 (1980).
- ²⁷Praxis shareware based on R. P. Brent, *Algorithms for Minimization Without Derivatives* (Prentice-Hall, Englewood Cliffs, 1973), Chap. 7.
- ²⁸Unpublished results.
- ²⁹S. I. Weissman, *Annu. Rev. Phys. Chem.* **33**, 301 (1982).
- ³⁰J. Casas-Gonzalez, S. M. Jacobsen, K. R. Hoffman, and W. M. Yen, in *Extended Abstracts* (Electrochemical Society of America, Phoenix, 1991), Vol. 91-2, p. 954.
- ³¹P. M. Selzer, in *Laser Spectroscopy of Solids*, edited by W. M. Yen and P. M. Selzer (Springer, Berlin, 1981), Chap. 4.
- ³²A. D. Trifunac, R. G. Lawler, D. M. Bartels, and M. C. Thurnauer, *Prog. Reaction Kinetics* **14**, 43 (1986).
- ³³V. G. Baryshevski, M. V. Korzhik, M. G. Livshitz, A. A. Tarasov, A. E. Kimaev, I. I. Mishkel, M. L. Meilman, B. J. Minkov, and A. P. Shkadarevich, in Ref. 17, Vol. 10, p. 26.
- ³⁴H. Eilers, U. Hömmerich, S. M. Jacobsen, W. M. Yen, K. Hoffman, and W. Jia, *Phys. Rev. B* **49**, 15505 (1994).
- ³⁵X. Wu, S. Huang, U. Hömmerich, W. M. Yen, B. G. Aitken, and M. Newhouse, *Chem. Phys. Lett.* **233**, 28 (1995).
- ³⁶C. Deka, M. Bass, B. H. T. Chai, and X. X. Chang, in Ref. 18, Vol. 13, p. 47.
- ³⁷B. H. T. Chai, Y. Shimony, C. Deka, X. X. Chang, E. Munin, and M. Bass, in Ref. 18, Vol. 13, p. 28.
- ³⁸T. J. Carrig and C. R. Pollock, in Ref. 18, Vol. 13, p. 34.
- ³⁹W. Jia, H. Liu, Y. Wang, U. Hömmerich, H. Eilers, K. Hoffman, and W. M. Yen, *J. Lumin.* **60&61**, 158 (1994).
- ⁴⁰*Modern Pulsed and Continuous-Wave Electron Spin Resonance*, edited by L. Kevan and M. K. Bowman (Wiley, New York, NY, 1990).
- ⁴¹Note added in proof: An electron spin-echo detection of several vibronic modes of photoexcited manganese doped in Ba₃(VO₄) has recently been reported by B. Buijsse, J. Schmidt, I. Y. Chan, and D. J. Singel, *Phys. Rev. B* **51**, 6215 (1995).